AJNR

Contrast-enhanced MR Angiography of Supraaortic Vessels: The Effect of Voxel Size on Image Quality

Xavier Leclerc, Lionel Nicol, Jean-Yves Gauvrit, Vianney Le Thuc, Didier Leys and Jean-Pierre Pruvo

AJNR Am J Neuroradiol 2000, 21 (6) 1021-1027
http://www.ajnr.org/content/21/6/1021

AJNR Am J Neuroradiol 21:1021–1027, June/July 2000

Contrast-enhanced MR Angiography of Supraaortic Vessels: The Effect of Voxel Size on Image Quality

Xavier Leclerc, Lionel Nicol, Jean-Yves Gauvrit, Vianney Le Thuc, Didier Leys, and Jean-Pierre Pruvo

BACKGROUND AND PURPOSE: **Several acquisition strategies may be used for imaging supraaortic vessels by using contrast-enhanced MR angiography. The purpose of this study was to assess the effect of voxel size on image quality of MR angiograms.**

METHODS: **Fourty-four patients underwent 3D MR angiography in the coronal plane. Patients were randomly assigned into two groups according to the voxel size of MR angiograms: group 1 referred to a 1.3 × 1.29 × 1.25-mm voxel size and group 2 to a 0.95 × 0.76 × 0.82-mm voxel size. Signal-to-noise ratios (SNRs) were measured and image artifacts were analyzed by consensus between observers. The delineation of the arterial lumen was independently ranked on a four-point scale (1 = not assessable; 2 = poor delineation; 3 = fair delineation; 4 = optimal delineation).**

RESULTS: **The overall interobserver agreement for the delineation of the arterial lumen was good ($\kappa = .84$, $P < .0001$), with a rank significantly higher in group 2 (68% of arteries graded as 4) compared with group 1 (76% graded as 3). SNRs were significantly higher by using the conventional resolution technique, with a negative correlation between SNRs and artery delineation ($P < .0001$). Image artifacts, however, were more frequent with the high-resolution technique, including wrap-around artifacts and signal fall-off at the origin of the great vessels.**

CONCLUSION: **MR angiograms with a decreased voxel size improve the delineation of cervical carotid and vertebral arteries, despite reduced SNRs and additional artifacts.**

Contrast-enhanced 3D MR angiography is widely used for imaging vascular structures such as the aorta (1), the renovascular system (2, 3), peripheral vessels (4), and, more recently, the supraaortic vessels (5−8). The principle is based on T1 shortening produced by the gadolinium chelate that provides high signal intensity in vascular structures. Compared with the time-of-flight (TOF) technique, contrast-enhanced MR angiography has some advantages. Contrast-enhanced MR angiography does not depend on the in-flow effect, providing angiographic images similar to those obtained by conventional catheter angiography. The short scan time minimizes motion artifacts and this enables performance of MR examinations in elderly people at the acute phase of stroke. Finally, the short echo time minimizes intravoxel dephasing artifacts related to disturbed flow, and this theoretically improves the evaluation of vascular occlusive disease. For an optimal arterial phase of contrast material enhancement, however, it is important to time the bolus of contrast agent so that the peak of maximal concentration of gadolinium in cervical arteries coincides with the acquisition of the central portion of k-space. The latter contains low spatial frequency information and determines the image contrast (9).

Despite the interest generated by contrast-enhanced MR angiography for imaging vascular structures, the evaluation of both the proximal portion of the supraaortic vessels and the distal segments of the carotid and vertebral arteries remains difficult (5, 6). This difficulty can be explained by the rapid venous enhancement in this region related to the blood-brain barrier, which prevents gadolinium extraction, by the change in surrounding structures between the lower and the upper portions of the cervical arteries, and by the wide range in size between the proximal great vessels and the upper portion of the cervical arteries. The small size of the vertebral arteries requires optimization of the spatial resolution, but the decreased voxel size leads to an inherent reduction in signal-to-noise ratio (SNR), which can degrade the overall image quality.

A preliminary study evaluating atherosclerotic disease of both the anterior and posterior circula-

Received October 12, 1999; accepted after revision January 10, 2000.

From the Departments of Neuroradiology (X.L., J.Y.G, V.L T., J.P.P.) and Neurology (D.L.), Hôpital Roger Salengro, University Hospital of Lille (France); and the Medical Division, Siemens (L.N), Saint-Denis (France).

Address reprint requests to X. Leclerc, MD, Service de Neuroradiologie, Hôpital Roger Salengro, Boulevard du Professeur Leclercq, 59037 Lille, France.

tions with contrast-enhanced MR angiography (6) showed several technical limitations such as imaging coverage, spatial resolution, and flow-related artifacts. The complete replacement of catheter angiography by MR angiography for the evaluation of cerebrovascular diseases remains the main challenge in the future. This requires high-performance gradients, specific coils, and appropriate sequences with trade-offs between spatial resolution, time resolution, acquisition volume, and SNR (5, 10, 11).

The aim of this study was to evaluate the image quality of contrast-enhanced MR angiography for the visualization of the cervical course of the carotid and vertebral arteries by using two different sequences that only differed by the spatial resolution.

Methods

Patients

From September to December 1998, 44 consecutive patients (24 men, 20 women; median age, 57 years [range, 43 to 90 years]) with suspected cerebrovascular disease were included in an ongoing study assessing the effect of voxel size on image quality of contrast-enhanced MR angiography for the visualization of supraaortic vessels. Informed consent was obtained in all cases for the 3D MR angiography examinations. All patients were assigned to one of the two groups in a randomized order. Spatial resolution of MR angiographic sequences was higher in group 2 compared with group 1. Each group included 22 patients with a mean age that did not differ significantly between the groups (group 1, 58 years; group 2, 55 years). One patient of group 1 and two patients of group 2 had acute dissection of the cervical arteries, six patients of group 1 and eight patients of group 2 were referred for an atherosclerotic disease and, in one patient of group 2, MR angiography was performed for the follow-up of a pseudoaneurysm of the internal carotid artery. In the remaining patients, MR angiograms showed no significant lesion of the supraaortic vessels.

Imaging Technique and Gadolinium Administration

All examinations were performed on a 1.5-T imaging system (Magnetom Vision; Siemens, Erlangen, Germany) with 25-mT/m maximum gradient strength. A transmitter-receiver, circular, polarized head-and-neck coil was used to assess the entire length of supraaortic vessels from their origins to the circle of Willis. After the patient was positioned within the coil with a 20-gauge intravenous catheter inserted into the antecubital vein, scout images were performed in three planes (axial, sagittal, and coronal) to program three pulse sequences as follows.

First, a test bolus was performed to evaluate individual contrast agent transit times. Continuously, sections were acquired every second at the C6 level for 50 seconds (TR/TE= 3.3/1.4, TI = 300, flip angle = 10°, matrix = 88 × 128, section thickness = 8 mm, field of view = 25). A bolus of 2 mL of gadolinium chelate (Gadodiamide Omniscan; Nycomed, Princeton, NJ) followed by 20 mL of normal saline was injected at the start of the sequence at a rate of 2 mL/sec by using an MR-compatible power injector (Spectris; Medrad, Pittsburg, PA). After completion, the transit time of the test bolus from the brachial vein to the carotid arteries was calculated by means of signal intensity measurements within the region-of-interest (ROI) placed in the common carotid artery. This transit time corresponds to the interval between acquisition of the first nonenhanced section of the sequence and the first section with enhanced arterial lumen.

TABLE 1: Comparison of parameters of the two gadolinium-enhanced MR angiographic sequences

	Group 1	Group 2
Patients	22	22
TR/TE	4.6/1.8	4.6/1.8
Flip angle	35°	35°
Matrix	190 × 256	205 × 512
Number of partitions	56	84
Rectangular field of view	6/8	4/8
Maximum field of view	33 cm	39 cm
Slab thickness	70 mm	70 mm
Oversampling	39%	24%
Acquisition time	43 sec	43 sec
Gadolinium dose	0.2 mmol/Kg	0.2 mmol/Kg
Injection rate	2 mL/sec	2 mL/sec

Note.—Group 1 = voxel size of 1.3 × 1.29 × 1.25 mm, group 2 = voxel size of 0.95 × 0.76 × 0.82 mm.

Second, a transverse 2D time-of-flight (TOF) sequence of the neck was acquired in the axial plane from the aortic arch to the skull base (27/9, flip angle = 50°, section thickness = 3 mm, field of view = 25, and matrix = 128 × 256). The scan time was 1 minute 30 seconds. A saturation band was placed over the intracranial dural venous sinuses to eliminate the venous signal from the cervical region. This sequence was used to guide the position of the 3D volume in order to include both carotid and vertebral arteries in the angiographic sequence.

Third, an MR angiographic sequence was acquired in the coronal plane. To image a large volume with a high-resolution technique without scan-time penalty, we used partial Fourier transform imaging with asymmetrical sampling of k-space (12). The number of phase-encoding steps was reduced in the slice direction, whereas the central part of k-space, including maximal concentration of low spatial frequencies, was fully sampled at 35% of the acquisition. We used the same imaging parameters in the two groups of patients except for those examinations related to the spatial resolution (Table 1). In group 1, we used an effective number of partitions of 56, a 6/8 rectangular field of view with a maximum dimension of 33 cm in the frequency-encoding direction, and a 190 (phase) × 256 (frequency) matrix. These parameters led to a voxel size of 1.30 (phase) × 1.29 (frequency) × 1.25 (slice) mm. In group 2, the effective number of partitions was 84 with a 4/8 rectangular field of view and maximum dimension of 39 cm in the frequency-encoding direction. A 205 × 512 matrix was used, leading to a voxel size of 0.95 × 0.76 × 0.82 mm. Others parameters were identical for the two groups (4.6/1.8, slab thickness = 70 mm, flip angle = 35°). To minimize wrap-around artifacts, an oversampling in the phase-encoding direction was used (39% in group 1, 24% in group 2) so that the overall number of lines in k-space was roughly the same for both the groups. The bandwidth was 390 Hz per pixel. The imaging time was 43 seconds in both groups. The two sequences were timed so that the peak of arterial contrast enhancement coincided with the acquisition of the central part of k-space. A bolus of 0.2 mmol/kg flushed with 20 mL of normal saline was injected with the power injector at a rate of 2 mL/s. Owing to the acquisition of the middle of the k-space at 35% of the sequence, the delay time from the start of the injection to the start to the acquisition was calculated as follows: Delay Time (s) = Test Bolus Transit Time (s) + 0.5 Injection Time (s) − 0.35 Acquisition Time (s).

Image Analysis

The overall image quality was judged on hard-copy films of the maximum intensity projection (MIP) displays by two

trained radiologists (X.L., J.Y.G.) by consensus. The observers were asked to detect the image artifacts and their consequence on image interpretation. Image artifacts included: motion artifact; wrap-around artifact; venous overlap; signal fall-off; inadequate coverage; and ring artifact. Motion artifact appeared as ghosts or smears in the phase-encoding direction. Wrap-around artifact appeared at the level of the aortic arch as a superimposed signal on the field attributable to the reduced field of view used in the phase-encoding direction. Venous overlap was related to a venous enhancement of jugular veins or brachiocephalic veins with superimposition of cervical arteries on MIP images despite multiple projections. Signal fall-off corresponded to a rapid reduction in signal intensity at the lower part of the imaging volume. Inadequate coverage was related to an inappropriate position of the 3D slab leading to exclude an arterial portion from the acquisition volume. Finally, ring artifact corresponded to a linear signal void in the center of the arterial lumen related to a rapid change of gadolinium concentration during the acquisition. Each artifact was graded as 1 (minor artifact without consequence on image interpretation) or 2 (major artifact preventing accurate analysis of arterial lumen).

Qualitative and quantitative evaluations were also performed. For the qualitative assessment, MR angiograms were reviewed in a blinded fashion by two independent examiners (X.L, J.Y.G.) who separately reviewed MR images in a fully randomized order. The observers graded the delineation of the arterial lumen by using a four-point scale (1 = not assessable; 2 = poor delineation of the arterial lumen owing to a major edge blurring; 3 = fair delineation of the arterial lumen despite a mild blurring of the arterial lumen; 4 = optimal delineation of the arterial lumen). Analysis was performed in six vascular regions: the proximal portion of great vessels (brachiocephalic artery, left common carotid artery, and left subclavian artery), the carotid bifurcations, the carotid siphons, the proximal segments of the vertebral arteries from their origin to C6 (V0/V1), the midportion of the vertebral arteries from C6 to C2 (V2), and the distal portion of the vertebral arteries from C2 to the basilar artery (V3/V4). For each vascular region, the analysis was focused on the arterial portion, which appeared normal. For the quantitative evaluation, the SNR was calculated on the individual partitions by the ROI technique. The SNR was defined as the mean value of signal intensity in the enhanced arterial lumen (S) divided by the standard deviation in the background (N). The SNR was obtained for each patient by using the largest ROI at the following three locations: the brachiocephalic artery, the proximal portion of the internal carotid artery, and the midportion of the vertebral artery.

Statistical Analysis

Statistical tests were used for the qualitative (delineation of the arterial lumen) and quantitative (SNR) assessments to compare the image quality according to voxel size.

For the qualitative assessment, the first step of the analysis consisted of an evaluation of the level of interobserver agreement for the categorization of the arterial lumen delineation by means of the (κ) statistic. Kappa values between .4 and .8 suggested a moderate-to-substantial agreement, and values higher than .8 indicated an excellent agreement. Using Fisher's exact test, the second step consisted of a comparison between the conventional and high-resolution techniques for the delineation of the arterial lumen (categorization using a four-point scale) for each of the seven arterial locations.

For the quantitative assessment, SNRs yielded by the two techniques were compared with the Mann-Whitney *U* test. The relation between SNR (proximal great vessels, carotid and vertebral arteries) and the corresponding delineation of the arterial lumen (proximal great vessels, carotid bifurcation, and midportion of the vertebral arteries) was assessed across techniques by using the Spearman's rank-order correlation test. *P* values lower than .05 were considered significant.

TABLE 2: Distribution of image artifacts of contrast-enhanced MR angiograms according to the voxel size

	MR Angiography*	
Artifacts	Group 1	Group 2
Motion	0	1
Wrap-around	0	4
Venous overlap	2	3
Signal fall-off	0	4
Inadequate coverage	2	2
Ring artifact	0	0

Note.—Data are given as numbers of examinations.

* Group 1 = voxel size of 1.3 × 1.29 × 1.25 mm, group 2 = voxel size of 0.95 × 0.76 × 0.82 mm.

Results

Overall Image Quality (Table 2)

The overall image quality was judged as optimal in most patients. No motion or wrap-around artifact was depicted on the angiograms obtained from group 1. In group 2 (decreased voxel size), patient motion resulted in minor image degradation in one examination and wrap-around artifacts were observed in four patients with large shoulders. In three cases, these artifacts were considered minor (no consequence on image interpretation) (Fig 1), whereas in one case, the superimposed image of shoulders at the level of the proximal portion of great vessels significantly degraded the image quality.

Arterial enhancement appeared optimal at the level of the carotid bifurcations in both groups without ring artifact. A rapid fall-off in signal intensity was observed in four patients of group 2 (Fig 2) at the level of the proximal portion of the great vessels, compared with the mid and the upper portions of the cervical arteries, but this did not prevent accurate analysis of images. A complete isolation of the arterial phase (no enhancement of venous structures) was achieved in 34 patients, whereas a mild or moderate enhancement of venous structures was observed in the remaining 10 patients (23%), including six from group 1 and four from group 2 (Fig 3). Venous overlap was observed in two patients of group 1 at the level of the internal carotid artery and in three patients of group 2 at the level of the proximal great vessels (Fig 2), and this significantly degraded the interpretation of image. In four patients (two from group 1 and two from group 2), the imaging coverage was not appropriate, leading to an exclusion of part of the carotid siphons from the imaging volume.

Qualitative Assessment

Of the six arterial regions examined by conventional and high-resolution angiography (44 patients), the overall interobserver agreement for the qualitative grading of image quality based on the delineation of the arterial lumen was good and sig-

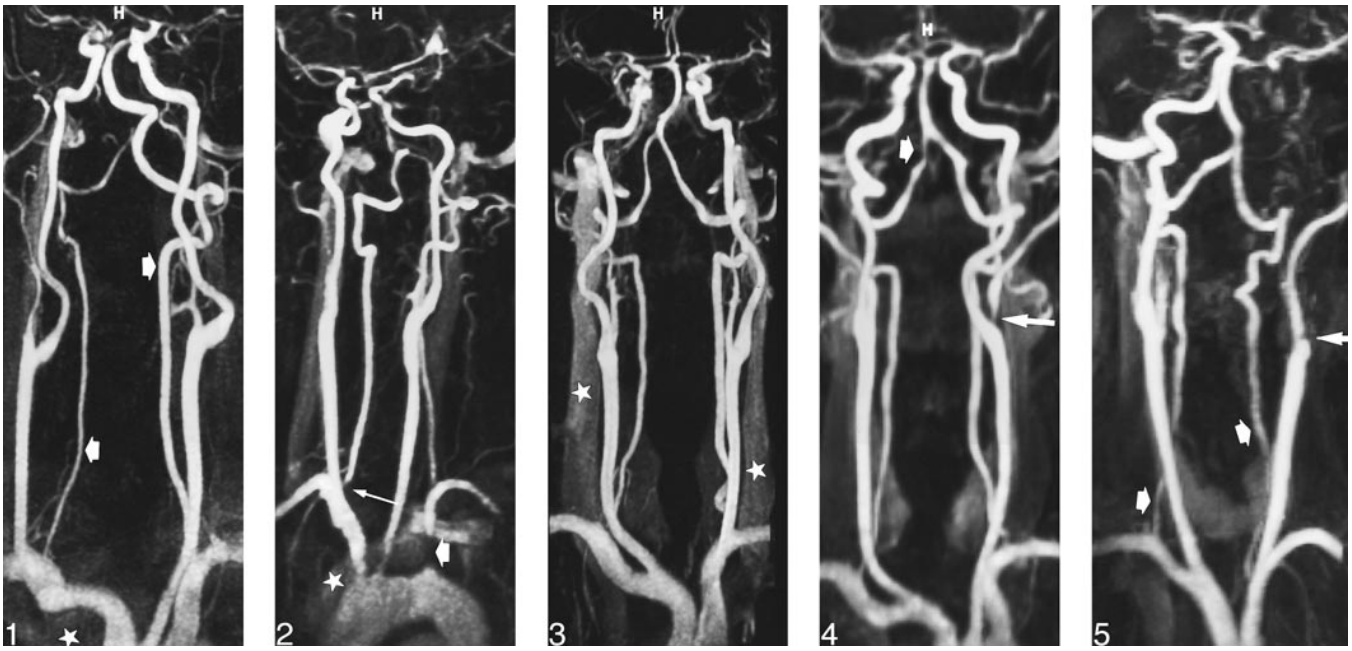

FIG 1. 46-year-old man referred for an ischemic event in the posterior fossa. Frontal view from contrast-enhanced MR angiogram (4.6/1.8/1, voxel size = 0.95 × 0.76 × 0.82) shows accurate delineation of vertebrobasilar system (*arrows*), despite wrap-around artifacts (*star*) at lower part of imaging volume that slightly degrade image quality.

FIG 2. 75-year-old man referred for a subclavian steal syndrome with occlusion of initial portion of left subclavian artery (*short arrow*) and stenosis at origin of right vertebral artery (*long arrow*). Oblique view from MR angiogram (4.6/1.8/1, voxel size = 0.95 × 0.76 × 0.82) shows a rapid fall-off of signal intensity at inferior part of imaging volume and a moderate enhancement of left brachiocephalic vein (*star*), which degrades image quality at level of aortic arch and at origin of great vessels.

FIG 3. 65-year-old man with atherosclerotic disease. Frontal view from MR angiogram (4.6/1.8/1, voxel size = 0.95 × 0.76 × 0.82) shows accurate delineation of cervical arteries, despite a moderate enhancement of jugular veins (*stars*).

FIG 4. 56-year-old man with left external carotid stenosis (*long arrow*) and severe short stenosis at the distal portion of the right vertebral artery (*short arrow*). Frontal view from MR angiogram (4.6/1.8/1, voxel size = 1.3 × 1.29 × 1.25) shows a fair delineation of artery outlines despite a slight blurring of arterial lumen.

FIG 5. 43-year-old woman with occlusive dissection of left internal carotid artery (*long arrow*). MR angiogram (4.6/1.8/1, voxel size = 1.3 × 1.29 × 1.25) shows a poor delineation of proximal segment of vertebral arteries (*short arrows*).

TABLE 3: Grading scale of contrast-enhanced MR angiograms according to the voxel size

		Grading Scale*			
Vascular Regions	Groups†	1	2	3	4
Proximal great vessels	Group 1	0	0	22	0
	Group 2	0	6	3	13
Carotid bifurcations	Group 1	0	4	18	0
	Group 2	0	0	1	21
Carotid siphons	Group 1	10	12	0	0
	Group 2	10	1	11	0
Vertebral arteries: V0/V1	Group 1	0	6	16	0
	Group 2	0	1	3	18
Vertebral arteries: V2	Group 1	0	0	22	0
	Group 2	0	0	4	18
Vertebral arteries: V3/V4	Group 1	0	0	22	0
	Group 2	0	0	2	20
Total	Group 1	10	22	100	0
	Group 2	10	8	24	90

Note.—Data are given as numbers of vascular regions.

* 1 = not assessable, 2 = poor delineation, 3 = fair delineation, 4 = optimal delineation.

† Group 1 = voxel size of 1.3 × 1.29 × 1.25 mm, group 2 = voxel size of 0.95 × 0.76 × 0.82 mm.

nificant ($\kappa = .84$, $P < .0001$). Nonetheless, discrepancies were observed in seven patients from group 1 and in 12 patients from group 2. These discrepancies mainly concerned the arterial portions at the extremes of the imaging volume (proximal great vessels, vertebral arteries [V0/V1], carotid siphons) and for the grades 3 (fair delineation) and 4 (optimal delineation) of the classification. Images that provoked disagreement between the observers were reevaluated in order to reach a consensus.

Comparisons between MR angiograms according the voxel size are shown in Table 3 (categorization). Overall delineation of the arterial lumen significantly differed across the voxel size for each vascular region (Fischer's exact test, $P < .0001$, all). Among the 132 regions examined in each group, 100 (76%) were graded as 3 in group 1 (Fig 4), whereas 90 (68%) were graded as 4 in group 2 (Fig 1). Carotid siphons were graded as 1 or 2 in all patients of group 1 and in half of patients of group 2. Proximal great vessels (brachiocephalic artery, left common carotid artery, and left subclavian artery) were better delineated in group 2, except in examinations of six patients in which arti-

TABLE 4: Findings of SNR (mean value, SD) measured in three ROIs according to the voxel size of MR angiograms

MR angiography*	ROI		
	Brachiocephalic Artery	Carotid Artery	Vertebral Artery
Group 1	61.2 (24.3)	156.7 (50.2)	90 (57.3)
Group 2	22.0 (6.2)	48.0 (11.1)	33.9 (9.0)

* Group 1 = voxel size of 1.3 × 1.29 × 1.25 mm, group 2 = voxel size of 0.95 × 0.76 × 0.82 mm.

facts degraded the image quality at the lower part of the imaging volume. The remaining arterial portions (carotid bifurcations and vertebral arteries) were significantly better delineated in group 2 as compared with group 1. Among the 66 arterial segments of the vertebral arteries examined in each group, six (9%) were graded as 2 in group 1 (Fig 5) and one (2%) in group 2.

Quantitative Assessment

The mean values of SNRs obtained in each group for the three ROIs are summarized in Table 4. SNRs appeared to be significantly higher in group 1 for all regions (Mann-Whitney *U* test, $P < .0001$). SNRs were lower at the level of the brachiocephalic artery as compared with the carotid and vertebral arteries (Wilcoxon rank-sum test, $P = .0001$ and $P = .0085$ respectively).

SNRs correlated negatively with the delineation grading scale (Spearman's rank-order correlation test, $P < .0001$, all), and this was related to the contrast between the decreased voxel size characterized by a better delineation and a lower SNR and the increased voxel size characterized by a lower delineation and a higher SNR.

Discussion

Our study showed that contrast-enhanced MR angiography of supraaortic vessels with a decreased voxel size provided a more accurate delineation of the arterial lumen. This allowed assessment of small vessels, such as the vertebral arteries, despite the presence of additional artifacts and the reduction in SNR. The main limiting factors concerned the reduction in signal intensity at the lower part of the coil, which could hinder the visualization of the proximal portion of the great vessels.

The MR angiographic sequence used in the present study constitutes a recent advance based on an asymmetrical sampling of k-space with a reduced number of phase-encoding steps in the slice direction. The central part of k-space that controls the image contrast was fully sampled during the first half of acquisition time. This allows either the improvement of temporal resolution by using continuous rapid acquisitions or improvement of the spatial resolution on a large volume by reducing the voxel size. We chose to optimize the spatial resolution and the volume coverage for the following reasons. First, among patients with atherosclerosis, the presence of atherosclerotic plaques at the origin of the great vessels or at the intracranial portion of the carotid arteries are not uncommon and may change the therapeutic strategy (13, 14). Second, the assessment of the vertebrobasilar system requires a large imaging volume and an optimal spatial resolution because of the length and the small size of the vertebral arteries (15). Finally, in young adults, cervical artery dissections are a frequent cause of stroke and may involve both the carotid and the vertebral arteries at multiple levels and this requires a complete visualization of supraaortic vessels (16).

The protocol used in the present study to obtain a voxel size less than 1 mm required a long scan time owing to the numbers of thin partitions in the 3D data set and the matrix size. This theoretically increased the risk of venous enhancement; however, despite a 43-second scan time, the venous structures were significantly enhanced in a minority of patients and remained slight or moderate. This can probably be explained by the short arterial phase and the sampling of low spatial frequencies at initial acquisition.

To maximize spatial resolution, a reduced field of view and a rectangular pixel, were used but this slightly degraded image quality obtained from some patients because of wrap-around artifacts at the lower part of the acquisition volume in the phase-encoding direction. We attempted to reduce this drawback by increasing the sampling points at each side of the field of view in the right-left direction. Wrap-around artifacts might be also minimized by using the subtraction technique that can suppress the signal intensity of the background tissue. This method is time-consuming, however, and does not provide a complete extinction of artifacts (17).

The anteroposterior coverage of 70 mm was appropriate in most of our patients to image the entire length of the carotid and the vertebral arteries. Nevertheless, the carotid siphons were excluded from the imaging volume in four patients. This could be explained by the 2D TOF images used to position the 3D slab, which did not cover the upper portions of the carotid arteries.

The image quality at the lower part of the acquisition volume was reduced in four patients by using a decreased voxel size with a rapid fall-off of signal intensity at the level of the proximal great vessels. This was probably related to the coil configuration and the frequent artifacts observed at the aortic arch level, including wrap-around artifacts, venous overlap, cardiac beat, and breath artifacts. Image quality might be improved by using a breath-hold technique that eliminates respiratory-induced ghost artifacts (5). Breath-hold acquisition, however, would have been difficult to apply in our study because of the long scan time it requires.

Despite a more accurate delineation of the cervical arteries achieved using a smaller voxel size, our findings showed that SNR decreased accordingly. The SNR is related to the voxel volume (V) according the following formula: $SNR = k \times V$, where k is a proportionality constant that depends on multiple parameters including magnetic field, coil configuration, longitudinal relaxivity, k-space sampling, repetition time, number of phase-encoding steps, and intravascular concentration of contrast agent. By combining a short repetition time, an oversampling, and an increased matrix size to obtain a voxel size less than 1 mm in the present study, the reduction in SNR appeared inevitable. To minimize this drawback, the concentration of gadolinium in cervical arteries during the acquisition of the center of k-space has to be improved. Our protocol of gadolinium administration was in agreement with the study of Kopka et al (18) that evaluated different injection rates by automatic power injection versus manual injection for the visualization of the abdominal aorta and its branches. It would, however, be useful to evaluate higher doses of gadolinium and higher injection rates to eliminate the reduction in SNR. Finally, a precise synchronization between the contrast agent infusion and the start of the acquisition was required to optimize the arterial phase of contrast enhancement. If the acquisition occurs too early, a misregistration may be observed, leading to ring artifacts (19). Conversely, if the acquisition occurs too late, the first-pass arterial enhancement can miss, with subsequent major venous enhancement. The timing of injection is important to define, especially in our protocol, because of the 10-second infusion duration that led to a short arterial phase. The scan delay was defined after a test bolus so that the peak of arterial phase enhancement coincides with 35% of the acquisition time. This provided optimal arterial phase of contrast enhancement in all patients. No major venous enhancement and no ring artifact were observed, and this was in agreement with previously published studies evaluating the effectiveness of a test bolus to calculate the transit time (20, 21). Errors might be theoretically observed when the cardiac output differs between the test and the angiographic sequence. Other effective methods have been described to time the start of data acquisition with the arrival of the contrast bolus. One technique automatically triggers the 3D angiographic sequence by continuously monitoring the signal intensity within a volume of interest (22–24). An automatic acquisition occurred when the defined threshold value is reached. A more recent technique consists of a manual-trigger 3D sequence obtained using a fluoroscopic 2D imaging (25), but this technique is not yet available on most magnets.

A drawback of the present study concerns the lack of conventional angiography to compare the effects of voxel size on image analysis. At our institution, we currently combine Doppler sonography and contrast-enhanced MR angiography at the acute stage of stroke to avoid the potential risk of complication of conventional angiography. When a discrepancy is observed between the two examinations, helical CT or conventional angiography is performed. Thus, among the 44 patients enrolled in the present study, only six underwent conventional angiography. For routine evaluation of carotid or vertebral stenosis, we usually generate contrast-enhanced MR angiograms with a reduced voxel size because this allows better estimation of the degree of stenosis, especially in cases of mild or moderate stenosis. When, however, a near-occlusive carotid stenosis or a stenosis at the proximal portion of great vessels is detected by Doppler sonography, a sequence including an increased voxel size may be more appropriate for avoiding the additional signal loss related to the reduced voxel size. Finally, in certain clinical conditions leading to a lower concentration of gadolinium in the arterial lumen such as hypertension, low cardiac output, or tortuous vessels, an increased voxel size may be theoretically preferable to improve the SNR.

Conclusion

Technical developments combining the partial sampling of k-space and a circular, polarized head-and-neck coil in the present study allowed MR angiography full coverage of cervical vasculature and a voxel size less than 1 mm. Our findings showed that the delineation of the artery outlines was more accurate when using a decreased voxel size. The reduction in SNR inherent to the increased spatial resolution, however, constituted the main limiting factor that requires specific coils, appropriate concentrations of contrast agent, and accurate bolus timing. Trade-offs between spatial resolution, acquisition time, and image contrast must be carefully chosen according to the clinical applications.

References

1. Prince MR, Narasimham DL, Stanley JC, et al. **Breath-hold gadolinium-enhanced MR angiography of the abdominal aorta and its major branches.** *Radiology* 1995;197:785–792
2. Siegelman ES, Gilfeather M, Holland GA, et al. **Breath-hold ultrafast three-dimensional gadolinium-enhanced MR angiography of the renovascular system.** *AJR Am J Roentgenol* 1997; 168:1035–1040
3. Bakker J, Beek FJ, Beutler JJ, et al. **Renal artery stenosis and accessory renal arteries: accuracy of detection and visualization with gadolinium-enhanced breath-hold MR angiography.** *Radiology* 1998;207:497–504
4. Ho KY, de Haan MW, Kessels AG, Kitslaar PJ, van Engelshoven JM. **Peripheral vascular tree stenoses: detection with subtracted and nonsubtracted MR angiography.** *Radiology* 1998;206: 673–681
5. Krinsky G, Maya M, Rofsky N, et al. **Gadolinium-enhanced 3D MRA of the aortic arch vessels in the detection of atherosclerotic cerebrovascular occlusive disease.** J *Comput Assist Tomogr* 1998;22:167–178
6. Leclerc X, Martinat P, Godefroy O, et al. **Contrast-enhanced three-dimensional with steady-state (FISP) MR angiography of supraaortic vessels: preliminary study.** *AJNR Am J Neuroradiol* 1998;19:1405–1413
7. Sardanelli F, Zandrino F, Parodi RC, De Caro G. **MR angiography of internal carotid arteries: breath-hold gd-enhanced 3D fast imaging with steady-state precession versus unenhanced 2D**

and 3D time-of-flight techniques. *J Comput Assist Tomogr* 1999; 23:208–215
8. Willig DS, Turski PA, Frayne R, et al. **Contrast-enhanced 3D MR DSA of the carotid artery bifurcation: preliminary study of comparison with unenhanced 2D and 3D time-of-flight MR angiography.** *Radiology* 1998;208:447–451
9. Mezrich R. **A perspective on K-space.** *Radiology* 1995;297–315
10. Rofsky NM, Adelman MA. **Gadolinium-enhanced MR angiography of the carotid arteries: a small step, a giant leap?** *Radiology* 1998;209:31–34
11. Remonda L, Heid O, Schroth G. **Carotid artery stenosis, occlusion, and pseudo-occlusion: first-pass, gadolinium-enhanced, three-dimensional MR angiography−Preliminary study.** *Radiology* 1998;209:95–102
12. Pipe JG. **Asymetric sampling along k slice-select in two-dimensional multislice MR imaging.** *Magn Reson Med* 1998;39: 625–634
13. The French Study of Aortic Plaques in Stroke Group. **Atherosclerotic disease of the aortic arch as a risk factor for recurrent ischemic stroke.** *N Engl J Med* 1996;334:1216–1221
14. Shuler JJ, Flanigan DP, Lim LT, Keifer T, Williams LR, Behrend AJ. **The effect of carotid siphon stenosis on stroke rate, death, and relief of symptoms following elective carotid endarterectomy.** *Surgery* 1982;92:1058–1067
15. Hoffmann M, Sacco RL, Chan S, Mohr JP. **Noninvasive detection of vertebral artery dissection.** *Stroke* 1993;24:815–819
16. Leys D, Lucas C, Gobert M, Deklunder G, Pruvo JPP. **Cervical-artery dissections.** *Eur Neurol* 1997;37:3–12
17. Yamashita Y, Mitsuzaki K, Ogata I, Takahashi M, Hiai Y. **Three-dimensional high-resolution dynamic contrast-enhanced MR angiography of the pelvis and lower extremities with use of a phased array coil and subtraction: diagnostic accuracy.** *J Magn Reson Imag* 1998;8:1066–1072
18. Kopka L, Vosshenrich R, Rodenwaldt J, Grabbe E. **Differences in injection rates on contrast-enhanced breath-hold three-dimensional MR angiography.** *AJR AJR Am J Roentgenol* 1998; 170:345–348
19. Ito K, Kato J, Okada S, Kumazaki T. **K-space filter effect in three-dimensional contrast MR angiography.** *Acta Radiologica* 1997;38:173–175
20. Kim JK, Farb RI, Wright GA. **Test bolus examination in the carotid artery at dynamic gadolinium-enhanced MR angiography.** *Radiology* 1998;206:283–289
21. Lentschig MG, Reimer P, Rausch-Lentschig UL, Allkemper T, Oelerich M, Laub G. **Breath-hold gadolinium-enhanced MR angiography of the major vessels at 1.0 T: dose-response findings and angiographic correlation.** *Radiology* 1998;208:353–357
22. Isoda H, Takehara Y, Isogai S, et al. **Technique for arterial-phase contrast-enhanced three-dimensional MR angiography of the carotid and vertebral arteries.** *AJNR Am J Neuroradiol* 1998; 19:1241–1244
23. Foo TKF, Saranathan M, Prince MR, Chenevert TL. **Automated detection of bolus arrival and initiation of data acquisition in fast, three-dimensional gadolinium-enhanced MR angiography.** *Radiology* 1997;203:275–280
24. Prince MR, Chenevert TL, Foo TKF, Londy FJ, Ward JS, Maki JH. **Contrast-enhanced abdominal MR angiography: optimization of imaging delay time by automating the detection of contrast material arrival in the aorta.** *Radiology* 1997;203: 109–114
25. Huston J, III Fain SB, Riederer SJ, Wilman AH, Berntein MA, Busse RF. **Carotid arteries: maximizing arterial to venous contrast in fluoroscopically triggered contrast-enhanced MR angiography with elliptic centric view ordering.** *Radiology* 1999; 211:265–273